Final Report

Physics of Complex Networks: Structure and Dynamics

Università degli Studi di Padova

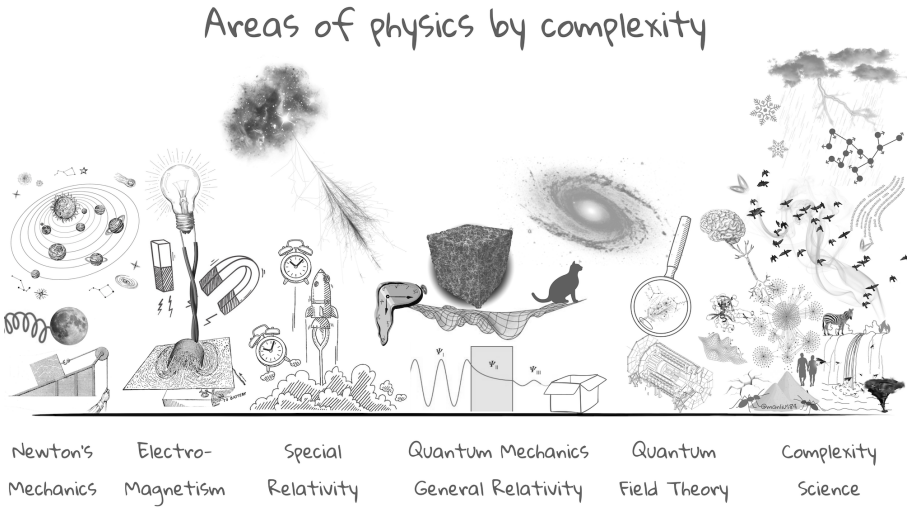

PoCN Project Report

Bettio, Vittoria

Last update: July 13, 2025

Contents

1 | Task 22: Epidemic spreading on temporal networks

1.1 | Task description

The goal of this project is to simulate classical epidemic models SIS, SIR and SEIR on temporal (time-evolving) networks. These models capture the dynamics of contagion processes and, when implemented on time-varying contact networks, allow for more realistic scenarios where interactions change over time.

1.2 | Mathematical Model

We consider a dynamic network of N agents (nodes), where each agent i is characterized by an *activity potential* $x_i \in [\epsilon, 1]$ drawn from a distribution $F(x)$ [5]. This activity potential represents the intrinsic tendency of node i to initiate interactions.

The *activity rate* a_i of node i is defined as:

$$a_i = \eta x_i,$$

where η is a normalization constant ensuring a desired average activity level across the system.

The network evolves in discrete time steps of duration Δt according to the following rules:

1. At each time step t, the network G_t starts with N disconnected nodes.
2. Each node i becomes *active* with probability $a_i \Delta t$. When active, it creates m links to m other nodes selected uniformly at random (inactive nodes can still receive connections).
3. All links are removed before the next time step; meaning that all interactions have a fixed duration Δt.

This construction generates a sequence of temporary-interaction networks, capturing the fast and heterogeneous nature of many real-world systems. We define the time-aggregated graph as the static network obtained by merging all connections that ever occurred over a given time window, assuming that all such links are simultaneously and permanently active.

Defining a Susceptible-Infected-Susceptible (SIS) dynamics on top of the evolving network, infection and recovery follow standard Markovian dynamics:

- An infected node recovers with probability $\mu\Delta t$.
- A susceptible node becomes infected with probability λ per contact with an infected node.

Let I_t^a be the number of infected individuals in the class of activity rate a at time t. The mean-field evolution equation for I_t^a is given by:

$$I_{t+\Delta t}^a = I_t^a - \mu\Delta t I_t^a + \lambda m\Delta t(N_a - I_t^a)a\frac{I_t}{N} + \lambda m\Delta t(N_a - I_t^a)\int da'\frac{I_t^{a'}a'}{N},$$

where N_a is the number of individuals with activity a, and $I_t = \int da\, I_t^a$ is the total number of infected nodes.

Neglecting higher-order terms and introducing $h(t) = \int da\, aI_t^a$, the evolution equations become:

$$\frac{dI}{dt} = -\mu I + \lambda m\langle a\rangle I + \lambda m h, \tag{1.1}$$

$$\frac{dh}{dt} = -\mu h + \lambda m\langle a^2\rangle I + \lambda m\langle a\rangle h. \tag{1.2}$$

The epidemic threshold $\beta_c = \lambda_c\langle k\rangle$ is obtained by linear stability analysis of the above system, [3] yielding:

$$\frac{\beta}{\mu} > \frac{2\langle a\rangle}{\langle a\rangle + \sqrt{\langle a^2\rangle}}. \tag{1.3}$$

This result highlights that the epidemic threshold depends on the first and second moments of the activity distribution, and not on the time-aggregated degree distribution. The validity of this analytical prediction is confirmed by our numerical simulations, as shown in Figure 1.2.

1.3 | Numerical Simulations

To validate the analytical insights, we implement Monte Carlo simulations of epidemic spreading on top of the activity-driven temporal network. Each node is assigned an activity potential x_i, sampled from a power-law distribution and rescaled to obtain an activity rate a_i. At every discrete time step, a new network is generated: each active node creates m links to randomly selected nodes, and all connections are removed before the next step.

The epidemic process is simulated using an agent-based, discrete-time Monte Carlo approach. For each node, state transitions occur probabilistically at each time step according to the parameters of the epidemic model (e.g., β infection rate, μ recovery rate, σ exposure rate). The considered models are SIS, SIR and SEIR.

Each configuration is simulated multiple times to account for stochastic variability. We compute time series of infected individuals and report aggregated statistics (median and standard deviation) to highlight qualitative trends and epidemic phases.

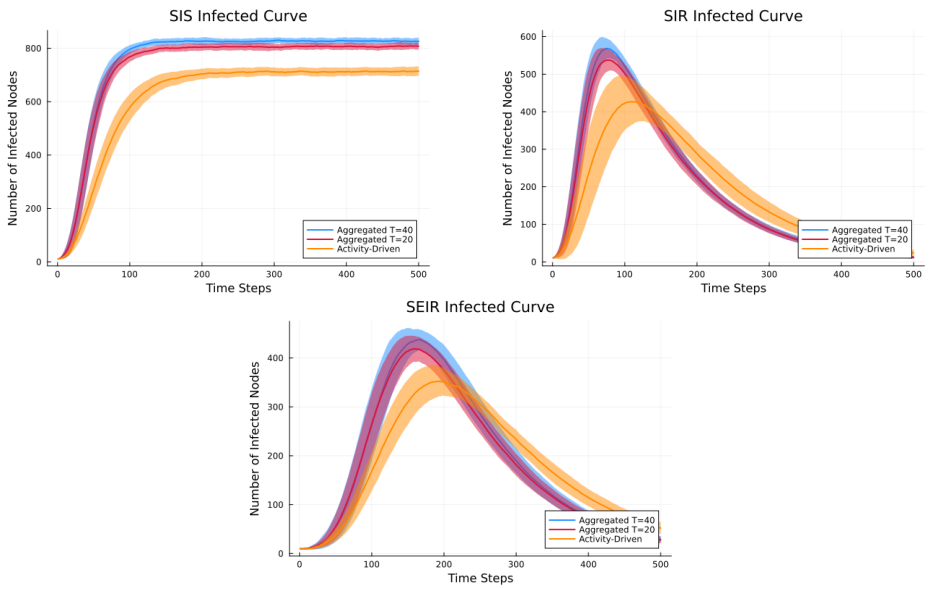

Figure 1.1: Epidemic peak comparison across different compartmental models and on three different network constructions: (i) the proposed temporal model, and (ii) its time-integrated versions over 20 and 40 time steps. Parameters: $N = 1000$, $\beta = 0.04$, $\mu = 0.01$, $\sigma = 0.04$, $m = 5$, $\eta = 10$, and the distribution $F(x) \propto x^{-\gamma}$ with exponent $\gamma = 2.1$ over the range $x \in [10^{-3}, 1]$ on 100 simulations.

On all three epidemic models (SIS, SIR, SEIR), we consistently observe in Figure 1.1 that the use of a temporal network leads to a **lower and delayed epidemic peak** compared to simulations performed on the corresponding time-aggregated network.

This behavior stems from the temporal sparsity of connections: at each time step, the network is highly fragmented, reducing the probability of transmission.

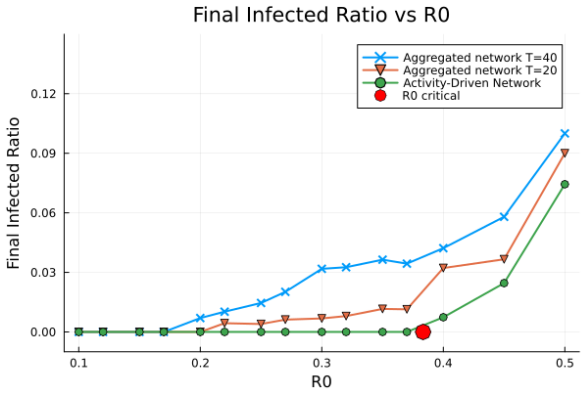

Figure 1.2: We display the stationary density of infected nodes I^*, obtained from Monte Carlo simulations of the SIS model on three different network constructions: (i) the proposed temporal model, and (ii) its time-integrated versions over 20 and 40 time steps. The parameters used are $N = 1000$, $m = 5$, $\eta = 10$, and $F(x) \sim x^{-\gamma}$ with $\gamma = 2.1$ and $x \in [10^{-3}, 1]$. Each data point represents the average over 100 independent simulations. The red dot indicates the analytically predicted critical reproductive number R_0^c in 1.3

1.4 | Appendix

To incorporate behavioral responses [4] to epidemic spread within the framework of Activity-Driven Temporal Networks, we introduced an **adaptive mechanism for the parameter** m, the number of links an active node generates. In this modified model, individuals reduce their connectivity based on the perceived infection level, effectively modeling a *fear-driven social distancing* response.

This adaptation is implemented through the following exponential relationship:

$$m(t) = m_0 \left(1 - e^{-\alpha I(t)}\right)$$

where:

- m_0 is the maximum number of links an active node creates;
- α is the adaptation strength, representing how sensitively individuals reduce contacts in response to infections;
- $I(t)$ is the global fraction of infected individuals at time t.

The dynamic is shown in Figure 1.3:

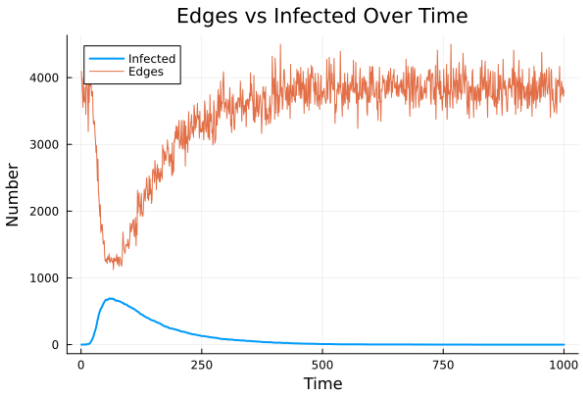

Figure 1.3: Temporal evolution of the number of infected individuals and total edges in the adaptive activity-driven network. As the number of infections rises, individuals reduce their connectivity, leading to a significant drop in the number of edges. As the epidemic subsides, contact activity gradually resumes.

This dynamic adaptation of m leads to two significant epidemiological consequences:

1. **Delayed and Flattened Epidemic Peaks** in Figure 1.4
   As the infection spreads and individuals perceive higher risk, they reduce their social activity (initiate fewer contacts). This **reduces the effective reproduction number in real time**, delaying the epidemic peak and lowering its height compared to the baseline case with fixed $m = m_0$. The result highlights how even simple behavioral feedbacks can substantially suppress transmission during the critical early phases of an outbreak.

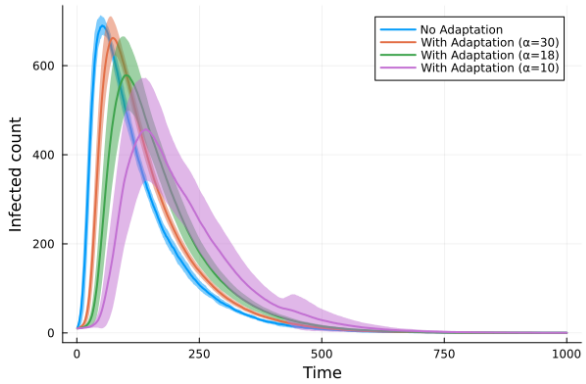

Figure 1.4: Epidemic curves under different strengths of adaptive behavior in an activity-driven temporal network.The parameters are $N = 1000, m_0 = 30, \eta = 10, \epsilon = 10^{-3}, \beta = 0.05, \mu = 0.01$. As the adaptation parameter α decreases, individuals become more responsive to perceived infection levels, reducing their contact activity more aggressively. This leads to a delayed and flattened infection peak.

2. **Emergence of Multiple Infection Waves** in Figure 1.5
   As infection levels decline, individuals gradually resume higher contact rates due to reduced perceived risk. This **behavioral relaxation** can reignite transmission, leading to **secondary (and possibly tertiary) waves** of infection. These waves emerge not from external factors, but from the **feedback loop** between perception-driven behavior and disease dynamics.

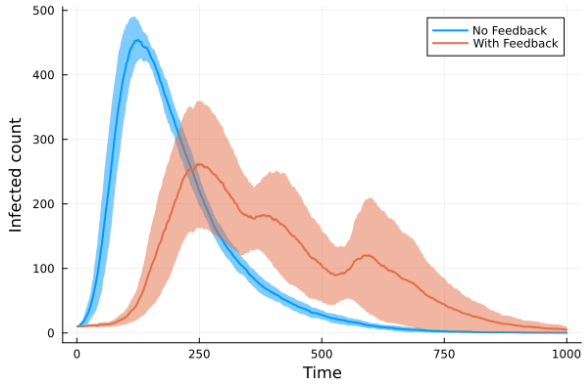

Figure 1.5: Comparison of infection dynamics with and without behavioral feedback in an activity-driven temporal network. Under specific parameter settings($N = 1000, m_0 = 20, \eta = 5, \epsilon = 10^{-3}, \alpha = 18, \beta = 0.04, \mu = 0.01$), the introduction of adaptive behavior leads not only to a reduction and delay of the initial peak, but also to the emergence of multiple waves of infection. These secondary peaks arise from the dynamic interplay between reduced connectivity during high infection periods and behavioral relaxation as perceived risk decreases.

This modeling approach captures more realistic epidemic trajectories, showing that adaptive contact behavior can influence both the intensity and temporal structure of outbreaks. Integrating fear-based feedback into temporal network models yields **richer dynamical outcomes** than static-contact assumptions, including **non-monotonic epidemic curves** and **complex collective responses**.

2 | Task 28: Voter Model

2.1 | Task Description

The objective of this project is to investigate how the degree distribution of a network influences the dynamics of the voter model. In particular, the study compares the temporal evolution of the interface density $\rho(t)$ in scale-free networks, characterized by broad degree heterogeneity, with that in single-scale networks (Erdős–Rényi or random regular graphs) that lack such heterogeneity. By isolating the effect of the degree distribution, the aim is to understand whether and how network heterogeneity accelerates or suppresses consensus formation.

2.2 | Mathematical Model

The voter model is a stochastic process used to study ordering dynamics and consensus formation in systems of interacting agents [2]. It is particularly suited for modeling opinion dynamics, where each agent can adopt one of two possible states, influenced by the states of its neighbors. The model is analytically tractable on regular lattices and provides rich phenomenology when implemented on complex networks.

Consider a network of N nodes, where each node i carries a binary variable $\sigma_i \in \{-1, +1\}$, representing one of two possible "opinions" or "states." The neighborhood of node i is denoted by $\mathcal{N}(i)$, and its degree is $k_i = |\mathcal{N}(i)|$.

The dynamics proceeds through asynchronous updates governed by interfacial noise:

1. At each elementary time step, a node i is selected uniformly at random.
2. A neighbor $j \in \mathcal{N}(i)$ is also chosen uniformly at random.
3. Node i adopts the state of node j: $\sigma_i \leftarrow \sigma_j$.

This update rule ensures that the dynamics is purely driven by local interactions and does not involve any energy minimization principle, unlike models such as the Ising model. The process continues until the system reaches an absorbing state or a metastable configuration.

The model has two absorbing states: full consensus where all $\sigma_i = +1$ or all $\sigma_i = -1$. Once such a state is reached, the dynamics halts. However, the path toward consensus depends strongly on the underlying network topology:

- In low-dimensional regular lattices (e.g., $d = 1$), the system undergoes domain coarsening and eventually orders.
- In complex networks with high dimensionality, heterogeneity, or randomness, the system often reaches a metastable disordered state that persists for long times before a rare fluctuation drives it to consensus.

To quantify the level of order in the system, we use the *interface density* $\rho(t)$, defined as the fraction of edges connecting nodes with opposite states [6]:

$$\rho(t) = \frac{1}{\sum_i k_i} \sum_{i=1}^{N} \sum_{j \in \mathcal{N}(i)} \frac{1 - \sigma_i \sigma_j}{2}.$$

This quantity satisfies:

- $\rho(t) \approx 1/2$ for a fully random initial state.
- $\rho(t) = 0$ in a fully ordered (consensus) state.
- A plateau $\rho(t) > 0$ indicates a metastable configuration.

2.3 | Numerical Simulations

We simulate the voter model on different network topologies—Barabási–Albert (BA), Erdős–Rényi (RN), and exponential (EN)—to study the effect of structure on the ordering dynamics. Each node carries a binary state $\sigma_i \in \{-1, +1\}$, updated asynchronously: at each step, a node adopts the state of a randomly chosen neighbor.

Networks of varying size ($N = 1000$ to 10000) with fixed average degree $\langle k \rangle = 8$ are generated. Simulations start from random initial conditions and evolve over time, recording the interface density $\rho(t)$, defined as the fraction of links connecting opposite spins. Results are averaged over many independent runs to reduce fluctuations.

2.1 shows the time evolution of the average interface density $\langle \rho(t) \rangle$ for the voter model on Barabási-Albert networks of various sizes. All simulations start from random initial conditions, with time measured in sweeps (i.e., N update steps). The initial value $\langle \rho(0) \rangle \approx 0.5$ reflects the uncorrelated state of spins.

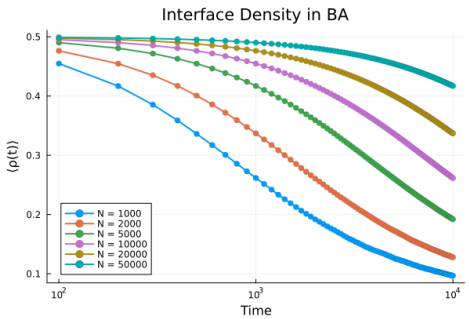

Figure 2.1: Time evolution of the average interface density $\langle \rho(t) \rangle$ for the voter model on Barabási-Albert networks with different system sizes N. Each curve represents the average over 1000 realizations on a network with average degree $\langle k \rangle = 6$.

As expected, smaller systems reach consensus more rapidly due to stronger finite-size fluctuations, resulting in a faster decay of $\langle \rho(t) \rangle$. In contrast, larger systems exhibit slower ordering dynamics and remain in partially ordered metastable states for longer times. This behavior illustrates the size dependence of the voter model's dynamics on scale-free networks and supports the known result that the survival time increases sublinearly with system size in these topologies.

2.2 compares the evolution of the average interface density $\langle \rho(t) \rangle$ in the voter model for three different network topologies: Barabási-Albert (BA), exponential (EN), and Erdős-Rényi (RN), across multiple system sizes. The results reveal that the network's degree distribution significantly impacts the ordering dynamics.

BA networks, which feature hubs due to their scale-free nature, reach consensus more rapidly as these highly connected nodes facilitate faster information spreading. In contrast, EN and RN networks, which have more homogeneous degree distributions, exhibit slower decay of $\langle \rho(t) \rangle$, indicating longer-lived metastable states.

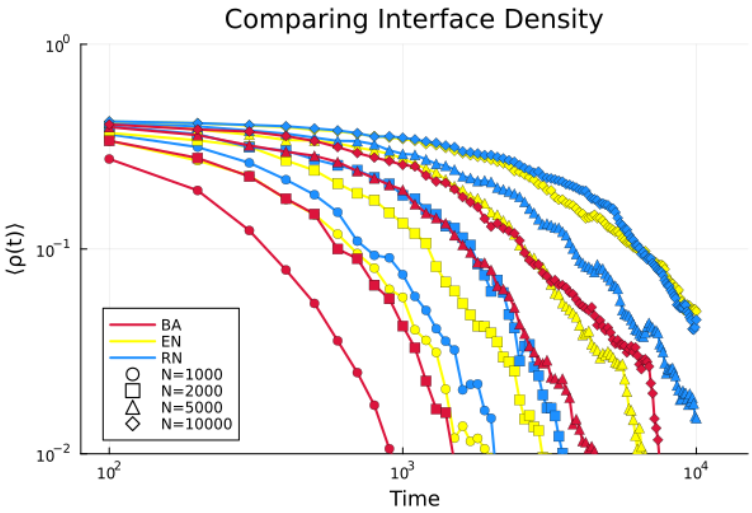

Figure 2.2: Comparison of the average interface density $\langle \rho(t) \rangle$ for the voter model on Barabási-Albert (BA), exponential (EN), and Erdős-Rényi (RN) networks, for various system sizes N. The average degree is fixed at $\langle k \rangle = 8$.

2.4 | Appendix

Figure 2.3 illustrates the evolution of the interface density $\rho(t)$ for 10 single realizations of the voter model on a Barabási–Albert network. All runs begin from random initial conditions and exhibit an initial decay, followed by a metastable plateau. During this phase, domain growth ceases and $\rho(t)$ fluctuates around a finite value.

Eventually, each trajectory collapses to the absorbing state ($\rho = 0$) at a different time, driven by spontaneous finite-size fluctuations. This behavior confirms the presence of long-lived metastable states in finite scale-free networks and illustrates the stochastic nature of the consensus process. The variability in collapse times underscores that the mean interface density $\langle(t)\rangle$ decays exponentially when averaged over many such realizations.

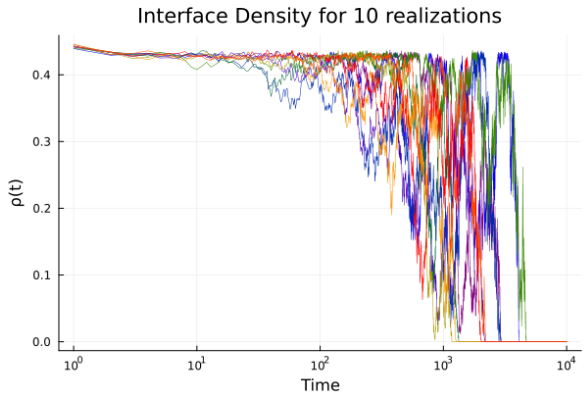

Figure 2.3: Interface density $\rho(t)$ for 10 independent realizations of the voter model on a Barabási–Albert network with $N = 10^4$ and average degree $\langle k\rangle = 8$. Each curve shows the evolution of a single realization. After a short transient, the system enters a metastable partially ordered state with finite ρ, which persists until a large fluctuation drives the system to consensus ($\rho = 0$). The distribution of consensus times highlights the stochastic nature of the ordering process in finite complex networks.

3 | Task 44: Social connectedness index from Facebook

3.1 | Task Description

The aim of this project is to construct a network representation of each country using the Facebook Social Connectedness Index (SCI) data [1]. The SCI quantifies the intensity of social ties between different geographic regions, based on anonymized data from active Facebook users and their friendship links.

For each country, a network is to be extracted where nodes correspond to subnational regions (e.g., NUTS3 regions in Europe, GADM levels elsewhere), and edges represent social connections weighted by the SCI. The SCI between two regions i and j is defined as:

$$\mathrm{SCI}(i,j) = \frac{FB_{connections}(i,j)}{FB_{users}(i) \cdot FB_{users}(j)}, \tag{3.1}$$

where $FB_{connections}(i,j)$ denotes the number of Facebook friendship ties between regions i and j, and $FB_{users}(i)$, $FB_{users}(j)$ are the number of users assigned to each region.

The geographic units used are based on the GADM (version 2.8) and NUTS 2016 classifications, depending on the country. The final output includes:

- A node file listing all regions with their corresponding geographic coordinates (latitude and longitude).
- An edge file containing the weighted connections between region pairs within the same country.

The resulting networks can serve as a basis for further analysis of intra-country social structures and spatial connectedness patterns.

3.2 | Methods

The construction and analysis of country-level social networks from Facebook Social Connectedness Index (SCI) data proceeded through several steps, combining data integration, spatial mapping, network building, and statistical analysis.

The main data source is the Facebook Social Connectedness Index (October 2021 release), provided in tab-separated format, listing SCI values between pairs of geographic units across the world. Each entry specifies a pair of regions identified by unique keys and the corresponding SCI.

To map each region key to a standardized geographic unit, we used a reference file containing region-level metadata, where each key is annotated with a region classification level (GADM1, GADM2, or NUTS3). Additional shapefiles were obtained using the `geodata` and `eurostat` R packages, to retrieve spatial geometries and centroids for each subnational unit.

All links involving the United States (which were overrepresented) were excluded. Only intra-country links were retained, ensuring that each country's network reflects internal social ties.

Regions were spatially matched based on their classification:

- For European countries with NUTS3 units, geometries and region names were matched using Eurostat's 2016 shapefiles.
- For other countries, GADM administrative units (levels 1 or 2) were used, downloaded via the `geodata` package.

Region centroids (longitude and latitude) were computed for each polygon to assign coordinates to the nodes in the resulting networks. Special care was taken to exclude regions with missing geometries or invalid centroids.

For each country, a social network was constructed where:

- Nodes represent subnational regions, annotated with a unique identifier, region name, and geographic coordinates.
- Edges represent social connections between region pairs, weighted by the SCI value.

Only region pairs within the same country were included. Node identifiers were assigned consistently across nodes and edges. The network is undirected, and loops and duplicate edges were excluded.

Two CSV files were produced for each country:

- `nodes.csv`: listing node IDs, names, and coordinates.
- `edges.csv`: listing pairs of connected node IDs, the SCI weight, and metadata (e.g., country name).

Each network was analyzed using the `igraph` R package.

Figure 3.1 reveals a clear quadratic relationship, consistent with the properties of nearly complete graphs: as the number of nodes increases, the number of edges increases approximately as $\sim N^2$, confirming that these national networks are densely connected.

There is a general negative correlation between average SCI and average degree 3.2: countries with higher SCI tend to have fewer connections per node, likely because

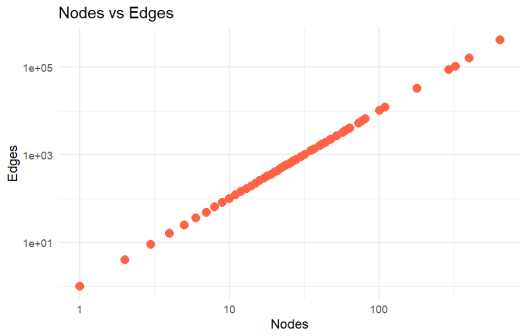

Figure 3.1: Scatter plot of the number of nodes versus the number of edges in each country's network. Both axes are shown on a logarithmic scale.

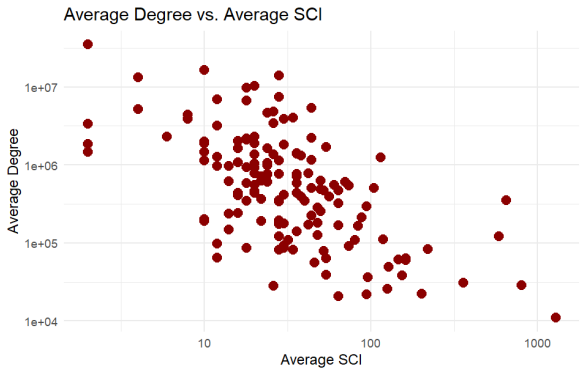

Figure 3.2: Scatter plot of the average node degree versus the average Social Connectedness Index (SCI) for each country's intra-national network. Both axes are on a logarithmic scale.

strong ties exist between fewer regions. This could reflect a more centralized or spatially clustered social structure.

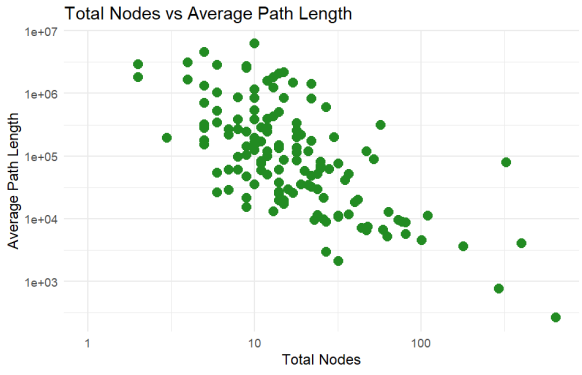

Figure 3.3: Scatter plot of the total number of nodes versus the average path length for each country, on a log-log scale.

As expected, countries with more nodes tend to exhibit lower average path lengths, indicating more densely connected and compact networks. However, the spread in Figure 3.3 suggests heterogeneity in the spatial distribution and strength of intra-country ties.

4 | Bibliography

[1] Facebook social connectedness index. https://data.humdata.org/dataset/social-connectedness-index, 2025. [Accessed 28 May 2025].

[2] Richard A Holley and Thomas M Liggett. Ergodic theorems for weakly interacting infinite systems and the voter model. *The annals of probability*, pages 643–663, 1975.

[3] Romualdo Pastor-Satorras, Claudio Castellano, Piet Van Mieghem, and Alessandro Vespignani. Epidemic processes in complex networks. *Reviews of modern physics*, 87(3):925–979, 2015.

[4] Nicola Perra, Duygu Balcan, Bruno Gonçalves, and Alessandro Vespignani. Towards a characterization of behavior-disease models. *PloS one*, 6(8):e23084, 2011.

[5] Nicola Perra, Bruno Gonçalves, Romualdo Pastor-Satorras, and Alessandro Vespignani. Activity driven modeling of time varying networks. *Scientific reports*, 2(1): 469, 2012.

[6] Krzysztof Suchecki, Víctor M Eguíluz, and Maxi San Miguel. Voter model dynamics in complex networks: Role of dimensionality, disorder, and degree distribution. *Physical Review E—Statistical, Nonlinear, and Soft Matter Physics*, 72(3):036132, 2005.